Structural, Spectroscopic and Theoretical Studies of a Diruthenium(II,II) Tetraformamidinate that Reversibly Binds Dioxygen

Sam Ring,[a] Anthony J. H. M. Meijer[a] and Nathan J. Patmore[b,*]

[a] *Department of Chemistry, University of Sheffield, Brookhill, Sheffield S3 7HF, United Kingdom*

[b] *Department of Chemical Sciences, University of Huddersfield, Queensgate, Huddersfield HD1 3DH, United Kingdom*

Email address: n.j.patmore@hud.ac.uk

Dedicated to Professor Malcolm Chisholm on the occasion of his 70th Birthday.

Abstract

The reaction of $Ru_2(O_2CMe)_4$ with *N,N′*-bis(3,5-dimethoxyphenyl)formamidine (Hdmof) in refluxing toluene solutions yields $Ru_2(dmof)_4$ as a diamagnetic red solid that is extremely air-sensitive. The crystal structure reveals the expected paddlewheel arrangement of ligands around the Ru_2^{4+} core, with a relatively long Ru-Ru bond (2.4999(8) Å) that is consistent with a $\sigma^2\pi^4\delta^2\pi^{*4}$ electronic configuration. This is supported DFT calculations that show this electronic structure results from destabilization of the δ^* orbital due to antibonding interactions with the formamidinate ligands. The cyclic voltammogram of $Ru_2(dmof)_4$ in a 0.1 M $^n Bu_4NPF_6$ / CH_2Cl_2 solution shows two redox processes, assigned as successive oxidations corresponding to the $Ru_2^{4+/5+}$ and $Ru_2^{5+/6}$ redox couples. Changes in the electronic absorption spectra associated with these oxidation processes were probed using a UV/vis spectroelectrochemical study. $Ru_2(dmof)_4$ reacts with dioxygen in solution to generate a purple compound that decomposes within an hour at room temperature. Bubbling N_2 gas through the purple solution regenerates $Ru_2(dmof)_4$, as evidenced by UV/vis spectrometry and cyclic voltammetry, suggesting that the dioxygen reversibly binds to the diruthenium core.

Keywords

Diruthenium, DFT, Spectroelectrochemistry, Electronic structure, Metal-metal bonds, Dioxygen

1. Introduction

Metal-metal multiply bonded diruthenium paddlewheel compounds have been shown to have potential application in a variety of areas, including molecular electronics [1], catalysis [2] and magnetic materials [3]. Part of the attraction of these compounds is the unique electronic structure that they posses, the precise nature of which is very dependant on the oxidation state of the metals and the identity of the metal bridging ligands [4]. Amidinate and anilinopyridinate (N,N) bridging ligands can stabilise Ru_2(III,III), Ru_2(II,III) and Ru_2(II,II) species that have proven to be of recent interest [5]. For example, Ren and co-workers have shown efficient electron transfer between, and through, diruthenium units using axially coordinated alkyne ligands [6]. In addition, Berry *et al.* have shown that *N*,*N*'-diphenylformamidinate diruthenium compounds with an axially coordinated azide ligand can undergo intramolecular C-H amination reactions [7].

By comparison to N,N bridged Ru_2^{6+} and Ru_2^{5+} compounds, much less is known about analogous Ru_2^{4+} paddlewheels. Recent studies by Jiménez-Aparicio and co-workers have shown that triazenate Ru_2^{4+} compounds can be synthesized by microwave techniques [8]. However this technique does not work for formamidinates, which are synthesized by the metathesis reaction of $Ru_2(O_2CMe)_4$ with the lithium formamidinate [9], by reduction of the corresponding Ru_2^{5+} tetraformamidinate by bulk electrolysis [10], or reduction with zinc [11]. Just four Ru_2^{4+} tetraamidinate complexes have been structurally characterized, two of which have no axial ligands and relatively long Ru-Ru bond distances (~2.46 Å) [9, 12]. The diamagnetic nature and long Ru-Ru bond lengths of these compounds suggest a $\sigma^2\pi^4\delta^2\pi^{*4}$ electronic configuration.

Reaction of diruthenium paddlewheel compounds with π-acceptor axial ligands often leads to decomposition to mononuclear species [13]. However, diruthenium paddlewheel compounds supported by N,N donor ligands are more resistant to decomposition. For example, $Ru_2(dpf)_4Cl$ and $Ru_2(dpf)_3(O_2CMe)Cl$ (dpf = *N,N'*-diphenyformamidinate) react with one or two equivalents of $NO_{(g)}$ and $NOBF_4$ to generate axial NO adducts with formal Ru_2^{4+}, Ru_2^{3+} and Ru_2^{2+} oxidation states [14]. Bear and Kadish have demonstrated that diruthenium(II,II) tetraamidinates can coordinate one CO ligand to the axial position, and the structures of $Ru_2(dpf)_4CO$ and $Ru_2(dpb)_4CO$ (dpb = *N,N'*-diphenylbenzamidinate) have been obtained [10, 15]. They display long Ru-Ru bond distances (2.5544(8) Å and 2.4789(8) Å respectively) indicating that the $\sigma^2\pi^4\delta^2\pi^{*4}$ electronic configuration has been retained by the diruthenium core.

In this study, we report the synthesis and structural characterization of a diruthenium tetraformamidinate, $Ru_2(dmof)_4$ (dmof = N,N'-bis(3,5-dimethoxyphenyl)formamidinate), and employ UV/vis spectroelectrochemistry and DFT calculations to probe the electronic structure. Reversible dioxygen binding to the diruthenium core in $Ru_2(dmof)_4$ was examined by UV/vis spectroscopy and cyclic voltammetry.

2. Results and discussion

2.1 Synthesis and characterisation

Ligand metathesis reactions of the Li or Na salt of the formamidinate ligand with $Ru_2(O_2CMe)_4$ can be used to generate diruthenium tetraformamidinates [9]. Initial attempts to synthesise $Ru_2(dmof)_4$ by this route were unsuccessful. MALDI-TOF mass spectra of the resulting product mixtures consistently showed the presence of the intermediate *bis* and *tris* substituted species

$Ru_2(O_2CMe)_{4-n}(dmof)_n$ (n = 2 or 3), in addition to the desired *tetrakis* compound. However, reaction of the protonated ligand with $Ru_2(O_2CMe)_4$ in refluxing toluene solutions did result in the clean isolation of $Ru_2(dmof)_4$, as shown in Scheme 1. The compound was isolated as an air-sensitive diamagnetic bright red solid that was characterized by NMR and IR spectroscopy and MALDI-TOF mass spectrometry.

Scheme 1. Reaction scheme for the formation of $Ru_2(dmof)_4$ and structure of the Hdmof ligand.

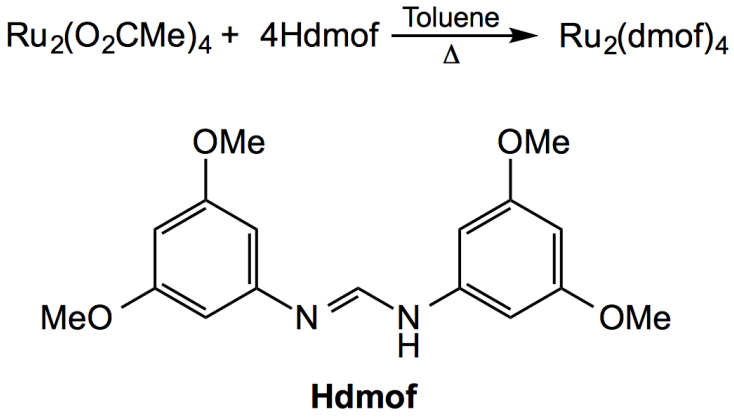

2.2 X-ray Crystallography

Crystals of $Ru_2(dmof)_4$ were obtained from a DCM / *n*-pentane layer at −18 °C. The crystal structure is shown in Figure 1, with selected bond lengths and angles given in Table 1. The formamidinate ligands bridge the dimetal core and adopt the expected paddlewheel arrangement with a Ru-Ru bond length of 2.499(8) Å. This is significantly longer than found for related diruthenium(II,II) tetracarboxylate compounds (Ru-Ru = 2.23-2.31 Å) [16] that have a $\sigma^2\pi^4\delta^2\delta^{*2}\pi^{*2}$ electronic configuration and a formal Ru-Ru double bond. It is consistent with the

proposed $\sigma^2\pi^4\delta^2\pi^{*4}$ electronic configuration for Ru_2(II,II) tetraformamidinates [9], in which the strongly antibonding π^* orbitals are populated in preference to the δ^* orbital. The Ru-Ru bond length for $Ru_2(dmof)_4$ is slightly longer than found for Ru_2(*p*-Me-$C_6H_4N\{CH\}NC_6H_4$-*p*-Me)$_4$ (2.475(1) Å) [9] and Ru_2(*p*-OMe-$C_6H_4N\{CH\}NC_6H_4$-*p*-OMe)$_4$ (2.4529(7) Å) [12].

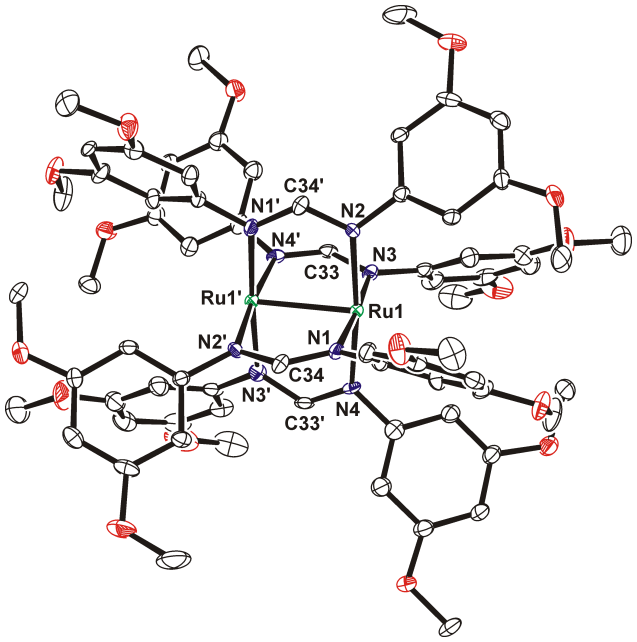

Figure 1. Crystal structure of $Ru_2(dmof)_4$ with hydrogen atoms omitted for clarity and thermal ellipsoids drawn at the 50% probability level. Atoms with an additional prime (') character are generated using the symmetry operation y, x, -z.

Table 1. Selected bond lengths (Å) and torsion angles (°) for $Ru_2(dmof)_4$.

Bond lengths			
Ru1-Ru1’	2.4999(8)	N1-C34	1.326(7)
Ru1-N1	2.028(5)	N2-C34’	1.333(7)
Ru1-N2	2.071(4)	N3-C33	1.337(7)
Ru1-N3	2.033(5)	N4-C33’	1.321(7)
Ru1-N4	2.069(4)		
Torsion Angles			
N1-Ru1-Ru1’-N2’	5.8(2)	N3-Ru1-Ru1’-N4’	5.6(2)

2.3 Computational Studies

In order to obtain a better understanding of the electronic structure of these compounds, we have performed DFT calculations on the model compound $Ru_2(dmf)_4$ (dmf = *N,N’*-diphenylformamidinate). The B3LYP functional has often been employed in computational studies on diruthenium paddlewheel compounds [17], although the use of alternative functionals has been probed more recently [18]. For modeling of related group 8 diiron and diosmium paddlewheel compounds, the Perdew-Burke-Ernzerhof exchange correlation functional (PBE0) has been found to perform well [19]. Geometry optimization of the singlet state of $Ru_2(dmf)_4$ was therefore performed using both B3LYP and PBE0 functionals, with the relativistic SDD basis set for ruthenium and 6-31G* for remaining atoms (see experimental section for further details). Selected bond lengths and torsion angles associated with the optimized structures using both functionals are shown in Table 2. Comparison of the experimental bond distances for $Ru_2(dmof)_4$ with the calculated structures shows that the PBE0 functional does a better job than B3LYP of modeling the diruthenium core geometry. Therefore, this functional will be used in the following discussion.

Table 2. Comparison of selected calculated bond lengths (Å) and torsion angles (°) for $Ru_2(dmf)_4$ with the experimental values for $Ru_2(dmof)_4$.

	B3LYP	**PBE0**	**$Ru_2(dmof)_4$**
Ru-Ru	2.518	2.494	2.4999(8)
Ru-N(average)	2.070	2.042	2.050
N-C{H}(average)	1.330	1.324	1.329
N-Ru-Ru-N(average)	6.5	6.1	5.7

A frontier MO energy diagram is shown in Figure 2, and selected orbital plots are shown in Figure 3. The HOMOs are the degenerate Ru_2-π^* orbitals, with the LUMO (Ru_2-δ^*) and LUMO+1 (Ru_2-σ^*) higher in energy by 2.45 eV and 3.51 eV. The MO plots show that the Ru_2-δ^* orbital is destabilized by antibonding interactions with the ligand nitrogen lone pairs, resulting in a $\sigma^2\pi^4\delta^2\pi^{*4}$ electronic configuration.

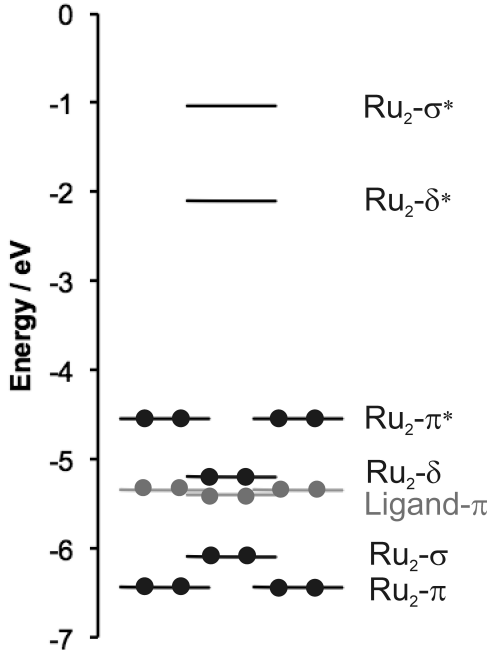

Figure 2. Calculated frontier MO energy level diagram for $Ru_2(C_6H_5N\{CH\}NC_6H_5)_4$.

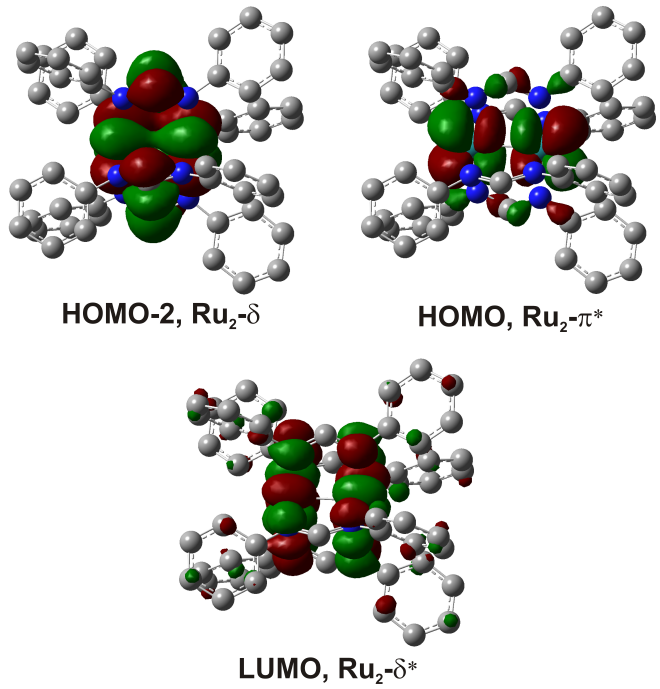

Figure 3. Selected MO plots for $Ru_2(C_6H_5N\{CH\}NC_6H_5)_4$ (0.02 isosurface value).

The first 30 optical transitions for $Ru_2(C_6H_5N\{CH\}NC_6H_5)_4$ were calculated using time-dependent DFT, and the results for transitions with $f > 0$ are displayed in Table 3. As expected for these types of compounds that have complicated electronic structures, there are a number of metal-metal and LMCT and MLCT transitions predicted to be observed in the UV/vis region, but only the ligand-π → Ru_2-δ^* LMCT transition at 613 nm and Ru_2-π/ligand-π → Ru_2-δ^* transition at 424 nm are likely to have significant intensity.

Table 3. Calculated transitions for $Ru_2(C_6H_5N\{CH\}NC_6H_5)_4$ with $f > 0$.

Energy (eV)	Wavelength (nm)	Oscillator strength (*f*)	Molar absorptivity (M^{-1} cm^{-1})[a]	Assignment
1.64	755	0.0092	360	Ru_2-π^* → Ru_2-σ^*
2.02	613	0.0688	2700	Ligand-π → Ru_2-δ^*
2.26	548	0.0052	200	Ru_2-δ → Ru_2-δ^*
2.92	424	0.1946	7630	Ru_2-π/Ligand-π → Ru_2-δ^*
3.06	405	0.0174	680	Ligand-π → Ru_2-σ^*
3.28	378	0.0086	340	Ru_2-π^* → Ligand-π^*

a) Assuming a Gaussian absorption with a peak-width at half-height of 3000 cm^{-1}.

2.4 Cyclic voltammetry and UV/vis spectroscopy

In a previous study, Ru_2(*p*-Me-$C_6H_4N\{CH\}NC_6H_4$-*p*-Me)$_4$ was found to display two redox processes at 0.713 and -0.568 V (*vs*. Fc/Fc^+), which were assigned as the $Ru_2^{4+/5+}$ oxidation and $Ru_2^{3+/4+}$ reduction, respectively [9]. The cyclic voltammogram recorded for $Ru_2(dmof)_4$ in dichloromethane is shown in Figure 4. Two reversible redox processes are observed at -0.584 V and 0.643 V. Based upon the results of the UV/vis spectroelectrochemical study, *vide infra*, we assign both of these processes as oxidations corresponding to the $Ru_2^{4+/5+}$ and $Ru_2^{5+/6+}$ redox couples, rather than an oxidation and reduction.

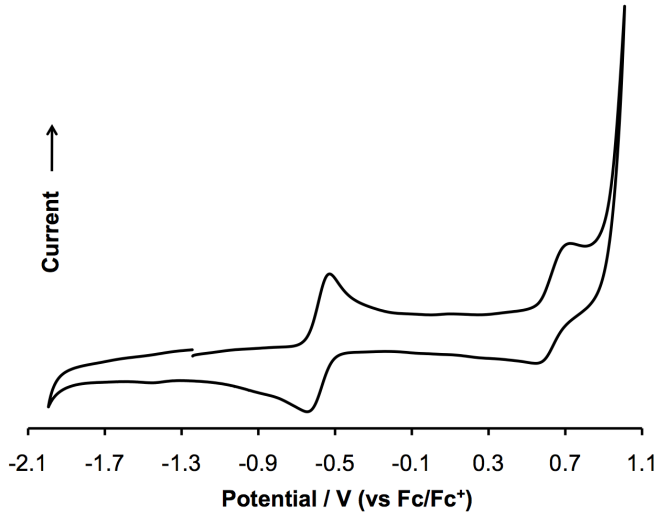

Figure 4. Cyclic voltammogram of $Ru_2(dmof)_4$ recorded in a 0.1 M $^nBu_4PF_6$ / CH_2Cl_2 solution at room temperature.

The UV/vis spectrum of $Ru_2(dmof)_4$ recorded in CH_2Cl_2 is shown in Figure 5 and displays a number of interesting features. There is a low energy transition observed at 888 nm, with at least four absorptions in the visible region at 548 (shoulder), 497, 432 and 399 nm. The lowest calculated singlet transition with any significant intensity is predicted to be at 613 nm, which is significantly higher in energy than the feature observed at 888 nm. In a detailed earlier study by Cotton and Ren [9] a similar disparity was found between the lowest calculated singlet transition for $Ru_2(HN\{CH\}NH)_4$ (employing SCF-Xα methods) and the experimentally observed feature at ~900 nm for $Ru_2(p\text{-}Me\text{-}C_6H_4N\{CH\}NC_6H_4\text{-}p\text{-}Me)_4$. This lead to assignment of this low energy transition as a $^3(Ru_2\text{-}\pi^* \rightarrow Ru_2\text{-}\delta^*)$ and $^3(Ru_2\text{-}\pi^* \rightarrow Ru_2\text{-}\sigma^*)$ absorption. Based upon the DFT results (Table 3), we tentatively assign the shoulder at 548 nm as Ligand-π → Ru_2-δ^* LMCT transition and the more intense absorption at 497 nm as Ru_2-π/Ligand-π → Ru_2-δ^*.

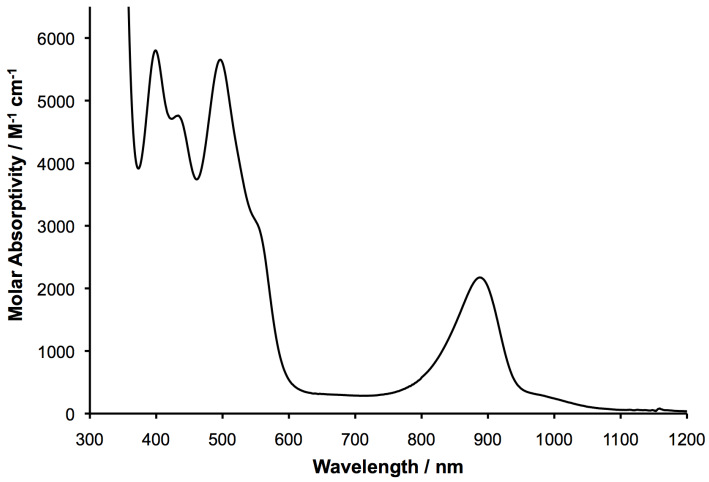

Figure 5. Electronic absorption spectrum of a 0.34 mmol solution of $Ru_2(dmof)_4$ recorded in dichloromethane.

2.5 UV/vis spectroelectrochemical studies

The spectral changes associated with the redox couples found in the cyclic voltammogram were probed using UV/vis spectroelectrochemical measurements. Holding the potential in the cell below -0.568 V results in no spectral changes, clearly indicating that this redox couple is the first oxidation potential.

The spectral changes associated with the $Ru_2^{4+/5+}$ and $Ru_2^{5+/6+}$ oxidations are shown in Figure 6. The first oxidation results in a loss in intensity of the transition at 888 nm, and growth of a new band at 723 nm. Reduction of the Ru_2^{5+} core to Ru_2^{6+} results in transition of this band to 854 nm. The spectral changes observed in the oxidation of $[Ru_2(dmof)_4]^+$ to $[Ru_2(dmof)_4]^{2+}$ are similar to those observed in the oxidation of $Ru_2(dpb)_4Cl$ [15].

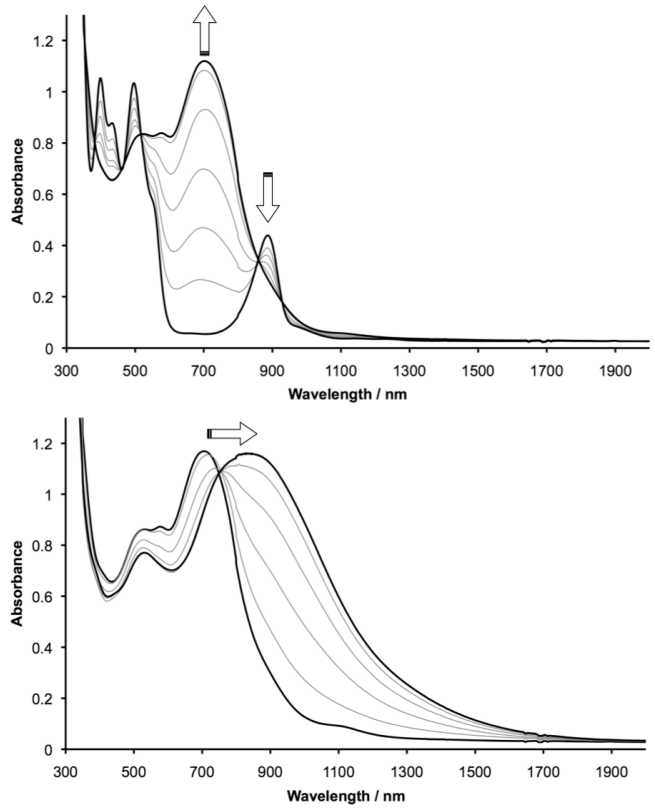

Figure 6. UV/vis/NIR spectroelectrochemical study of a 1.3 mmol solution of $Ru_2(dmof)_4$ in 0.1 M $^{n}Bu_4NPF_6$ / CH_2Cl_2 at room temperature. Spectral changes associated with the $Ru_2^{4+} \rightarrow Ru_2^{5+}$ oxidation are shown on top, and those associated with the $Ru_2^{5+} \rightarrow Ru_2^{6+}$ oxidation on the bottom.

2.6 Reversible reaction of $Ru_2(dmof)_4$ with dioxygen

Binding of dioxygen by metal complexes has received significant attention from synthetic chemists because of its relevance to the transport and activation of molecular oxygen in biological systems [20], and the insight it provides into possible mechanisms for oxidation catalysts [21]. As observed previously for diruthenium(II,II) tetraformamidinates [9], solutions of

$Ru_2(dmof)_4$ turn purple immediately upon exposure to air due to reaction with dioxygen. These purple solutions decompose within an hour at room temperature, and within 8 hours at -18°C, to give black solutions. Optical changes arising from exposure of CH_2Cl_2 solutions of $Ru_2(dmof)_4$ to dry O_2 gas were monitored by UV/vis spectroscopy (Figure 7). The resulting product displays a single intense absorption in the visible region at 549 nm, along with numerous weak absorptions that extend into the NIR region. Interestingly, bubbling N_2 or argon gas through the cell shortly after dioxygen addition results in regeneration of $Ru_2(dmof)_4$.

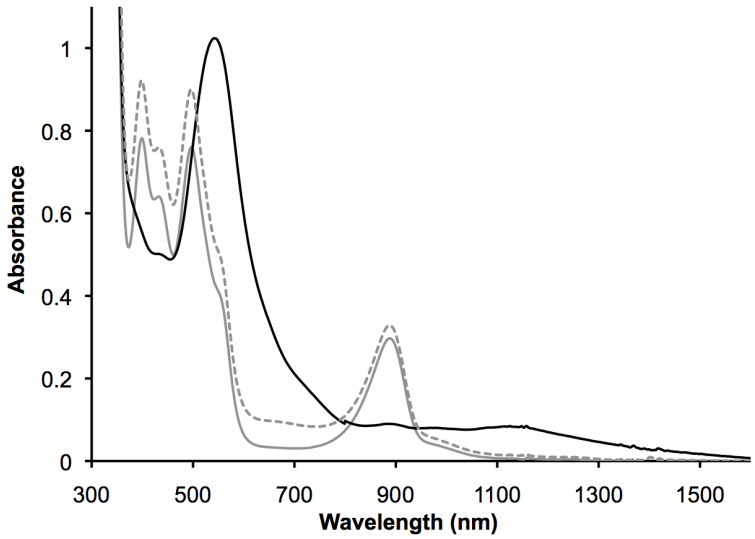

Figure 7. UV-vis spectra of a 0.34 mmol solution of $Ru_2(dmof)_4$ in CH_2Cl_2 before (grey line) and after (black line) exposure to dioxygen. The dotted line shows the spectrum obtained after bubbling argon through the cell for 5 minutes.

The reversible reaction with dioxygen suggests that it is axially binding to the complex, rather than generating mono- or di-nuclear oxo products. This is similar to the observed reactivity of

diruthenium tetraformamidinate with CO previously by reported by Bear and Kadish [10, 15]. Furthermore, the significant spectral changes suggest a major perturbation in the electronic structure of the diruthenium core, and oxidation to Ru_2^{5+} with a corresponding a superoxide ligand.

The cyclic voltammogram of the dioxygen product generate by bubbling O_2 through the cell is shown in Figure 8. The $Ru_2^{4+/5+}$ redox couple is now irreversible, but the original voltammogram is once more regenerated after bubbling nitrogen through the electrochemical cell.

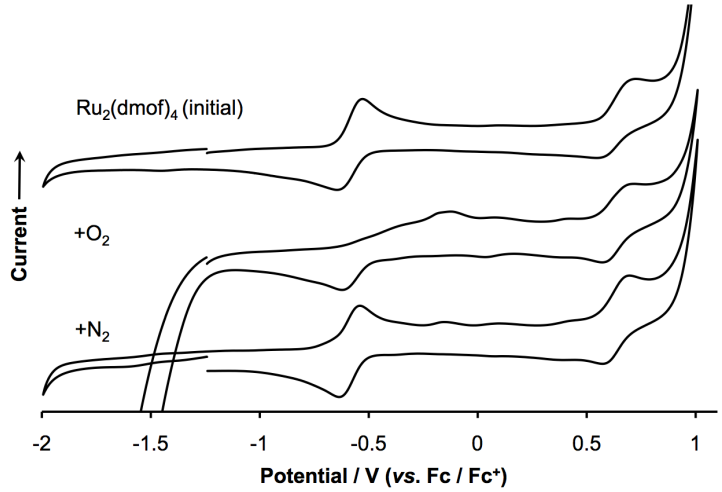

Figure 8. Cyclic voltammogram (0.1M $^{n}Bu_4NPF_6$ / CH_2Cl_2) of $Ru_2(dmof)_4$ before (top) and after (middle) exposure of the cell to O_2 gas. The bottom voltammogram was obtained by bubbling N_2 through the cell after the addition of O_2.

Despite numerous attempts, at room temperature and -18°C, we were unable to obtain crystals of the dioxygen product suitable for X-ray diffraction due to product decomposition in solution. Attempts to identify a superoxide adduct were made using IR spectroscopy. The lack of a solid-state structure for the $Ru_2(dmof)_4$ dioxygen adduct makes it difficult to definitively assign the

nature of this species. The expected weak O-O stretch was not observed in the IR spectrum due to the presence of strong ligand stretches in the expected region (1050 -1250 cm^{-1} [22]). Furthermore, solid-state magnetic susceptibility and Evans NMR (CD_2Cl_2) of the dioxygen product did not show evidence of paramagnetism, and no signals were observed in the EPR spectrum (solid state and CH_2Cl_2 solution) at room temperature.

3. Conclusions

The solid-state structure of diamagnetic $Ru_2(dmof)_4$ displays a relatively long Ru-Ru bond length consistent with the four previously reported structures of diruthenium(II,II) tetraamidinates, and a $\sigma^2\pi^4\delta^2\pi^{*4}$ electronic configuration. The cyclic voltammogram of $Ru_2(dmof)_4$ displays two redox processes, which were assigned as successive oxidations associated with the $Ru_2^{4+/5+}$ and $Ru_2^{5+/6+}$ redox couples. The low potential (-0.568 V) of the first oxidation accounts for the extremely air-sensitive nature of these compounds. $Ru_2(dmof)_4$ reacts quickly with dioxygen in solution, although the purple product decomposes in less than an hour at room temperature, preventing its structural characterization by X-ray crystallography. However, UV/vis spectroscopy and cyclic voltammetry indicates that $Ru_2(dmof)_4$ reversibly binds dioxygen, suggesting formation of an axially coordinated O_2 adduct.

4. Experimental

4.1 Physical methods

^{1}H and ^{13}C NMR spectra were collected at room temperature on a Bruker Avance 400 spectrometer, with chemical shifts assigned relative to the residual solvent peaks. Mass spectra were obtained either by ESI or MALDI-TOF-MS as indicated. ESI spectra were collected on a Waters Premier LCT operating in ESI mode. MALDI-TOF-MS spectra were obtained using a Bruker Reflex III mass spectrometer operating in positive ion mode using an N_2 laser, employing DCTB (trans-2-[3-(4-tert-Butylphenyl)-2-methyl-2-propenylidene]malononitrile) as the matrix.

Electrochemical measurements were conducted using an Metrohm Autolab PGSTAT100 potentiostat-galvanostat in a nitrogen purged 0.1M solution of [$^{n}Bu_4N$][PF_6] in CH_2Cl_2 using a standard three electrode system. This consisted of a polished Pt microdisc working electrode, Pt wire counter electrode, and an Ag/AgCl pseudo reference electrode; all potentials are given relative to the $FeCp_2/FeCp_2^+$ redox couple obtained by addition of a small amount of ferrocene into the cell at the end of the experiment. UV-Vis-NIR spectra were recorded using a Varian Cary 5000 spectrophotometer equipped with a 1 mm path length quartz cuvette. The UV/vis spectroelectrochemical studies were performed in an optically transparent thin layer electrode cell, in 0.1 M [$^{n}Bu_4N$][PF_6] / CH_2Cl_2 solutions, with a cell setup previously described by Ward and coworkers [23]. The dioxygen adduct was prepared for the electrochemistry and spectroscopic measurements by purging the cell with O_2 gas for 30 seconds. $Ru_2(dmof)_4$ was regenerated by bubbling dinitrogen gas through the solutions for 5 minutes.

Infrared spectra were obtained using either as solid samples with a Perkin-Elmer Spectrum RX I FT-IR spectrometer equipped with a DuraSamplIR II diamond ATR probe and universal press; or

as a solution in CH_2Cl_2 using a Perkin-Elmer Spectrum One FT-IR spectrometer in a quartz glass cell. Elemental analysis was conducted by the Microanalytical Service of the University of Sheffield, Department of Chemistry using a Perkin-Elmer 2400 Series II CHNS/O Analyser.

4.2 Materials

All manipulations involving diruthenium compounds were conducted using standard Schlenk-line techniques or in a glovebox under an inert atmosphere of argon. Toluene, *n*-pentane and CH_2Cl_2 were purified by distillation over CaH_2. $Ru_2(O_2CMe)_4$ was synthesised according to literature procedures [24], and all other reagents were obtained commercially and used without any further purification.

4.3 Synthesis of N,N'-bis(3,5-dimethoxyphenyl)formamidine (Hdmof)

A 100 mL round bottom flask was charged with 3,5-dimethoxyaniline (4.14 g, 27 mmol) and anhydrous triethyl orthoformate 2.33 mL (14 mmol), then fitted with a reflux condenser. The mixture was then heated to reflux for a period of 3 hours, after which the condenser was removed and the mixture boiled to dryness. The resultant solid was then purified by recrystallization from minimal volume of hot toluene (3.71 g, 12 mmol, Yield: 87 %). ^{1}H NMR ($CDCl_3$, 400 MHz): δ 3.72 (s, 12H), 6.19-6.23 (m, 6H), 8.25 (s, 1H), 9.84 (s, 1H). ^{13}C NMR ($CDCl_3$, 250 MHz): δ 55.3, 95.9, 97.5, 147.2, 149.8, 161.6. ESI-MS: calcd. monoisotopic *m/z* for $C_{17}H_{20}N_2O_4$: 316.14, found: 316.13 (M+, 100%). IR (cm^{-1}): 3342w, 2997w, 2938w, 2840w, 1664s, 1580s, 1513m, 1456m, 1423m, 1317m, 1281m, 1243m, 1191s, 1143s, 1062s, 1001s, 958m, 940m, 812s, 794s, 740m,

667s. Elemental analysis calcd. for $C_{17}H_{20}N_2O_4$: C, 64.54; H, 6.37; N, 8.86. Found: C, 64.35; H, 6.39; N, 8.79 (%).

4.4 Synthesis of $Ru_2(dmof)_4$

A Schlenk flask fitted with a reflux condenser was charged with $Ru_2(O_2CMe)_4$ 0.065 g (0.15 mmol), Hdmof (0.195 g, 0.62 mmol) and 20 mL of toluene. The resultant mixture was heated at reflux for 48 hours, then allowed to cool to room temperature and filtered through celite. The filtrate was reduced to minimum volume, and the product precipitated from solution by addition of *n*-pentane. The resulting bright red solid was then isolated by filtration, washed with a further 2 x 5 mL aliquots of *n*-pentane and dried *in vacuo*. (0.126 g, 0.086 mmol, Yield: 57 %). Crystals of $Ru_2(dmof)_4$ suitable for X-ray diffraction were grown by vapour diffusion of pentane into a DCM solution at -18°C over a period of several days. The product is extremely air-sensitive preventing the acquisition of a satisfactory elemental analysis. MALDI-TOF-MS: calcd. monoisotopic *m/z* for $Ru_2C_{68}H_{76}O_{16}N_8$: 1464.30, found m/z: 1464.31 (M+, 100%). ^{1}H NMR (CD_2Cl_2, 400 MHz): δ 3.74 (s, 48H, ArOC*H*$_3$), 5.97 (s, 8H, *p*-Ar*H*), 6.20 (d, 16H, o-Ar*H*), 8.19 (s, 4H, NC{*H*}N). IR, CH_2Cl_2 solution (cm^{-1}): 836 (w), 1066 (m), 1154 (s), 1194 (m), 1205 (s), 1339 (w), 1363 (w), 1395 (w), 1419 (w), 1424 (w), 1440 (w), 1457 (m), 1464 (m), 1472 (m), 1490 (w), 1507 (m), 1535 (s, sh), 1539 (s), 1559 (m), 1597 (s), 1653 (m), 1684 (m), 2311 (m sh), 2322 (m br), 2364 (m br). UV-vis, CH_2Cl_2 [λ_{max}, nm (ε, M^{-1} cm^{-1})]: 399 (5720); 432 (4688); 497 (5560); 548 (sh); 888 (2174).

4.5 X-ray crystallography

Data was measured on a Bruker Smart CCD area detector with Oxford Cryosystems low temperature system. After integration of the raw data and merging of equivalent reflections, an empirical absorption correction was applied (SADABS).[25] The structure was solved by direct methods (SHELXS-97) and refined by full- matrix least squares on weighted F^2 values for all reflections using the SHELX suite of programs.[26] All hydrogens were included in the models at calculated positions using a riding model with U(H) = 1.5 x U_{eq} (bonded carbon atom) for methyl hydrogens and U(H) = 1.2 x U_{eq} (bonded carbon atom) for aromatic hydrogens. The pentane solvent molecule is located on a centre of inversion and was modeled as being delocalized over two positions.

Crystal data for $Ru_2(dmof)_4 \cdot C_5H_{12}$. $C_{73}H_{88}N_8O_{16}Ru_2$, M = 1535.65, tetragonal space group $P4_12_12$, a = 11.3950(3) Å, c = 52.4067(15) Å, V = 6804.8(3) Å^3, Z = 4, D_{calc} = 1.499 Mg/m^3, μ = 0.520 mm^{-1}, 127548 reflections measured, 7813 unique (R_{int} = 0.0395) were used in all calculations. The final R_1 was 0.0593 (> 2σ(I)) and wR_2 was 0.1387

4.6 DFT calculations

DFT calculations were performed using the Gaussian09 suite of programs.[27] Calculations were performed using either the B3LYP[28] functional or Perdew–Burke–Ernzerhof exchange correlation functional (PBE0),[29] in combination with the effective core potential basis sets SDD[30] for Ru, and 6-31G* basis set[31] for all other atoms. Geometry optimisations were performed in the gas phase with C_4 (B3LYP) and D_4 (PBE0) symmetry constraints. Structures were confirmed to be minima on the potential energy surface by frequency analysis, and the

electronic absorption spectra was calculated using the time-dependent DFT (TD-DFT) method [32].

Acknowledgement

The work described in this paper was supported by a Royal Society University Research Fellowship (N.J.P.) and the E-futures doctoral training centre at the University of Sheffield (S.R.). All calculations were performed on the 'Sol' computer cluster of the Theoretical Chemistry group at the University of Sheffield.

Appendix A. Supplementary data

CCDC 1412563 contains the supplementary crystallographic data for $Ru_2(dmof)_4 \cdot C_5H_{12}$. This data can be obtained free of charge via http://www.ccdc.cam.ac.uk/conts/retrieving.html, or from the Cambridge Crystallographic Data Centre, 12 Union Road, Cambridge CB2 1EZ, UK; fax: (+44) 1223 336 033; or e-mail: deposit@ccdc.cam.ac.uk.

References

[1] a) D. Olea, R. González-Prieto, J. L. Priego, M. C. Barral, P. J. de Pablo, M. R. Torres, J. Gómez-Herrero, R. Jiménez-Aparicio, F. Zamora, *Chem. Commun.*, **2007**, 1591; b) J.-L. Zuo, E. Herdtweck, F. E. Kühn, *J. Chem. Soc., Dalton Trans.*, **2002**, 1244; c) M. Manowong, E. V. Caemelbecke, M. S. Rodriguez-Morgade, J. L. Bear, K. M. Kadish, T.

Torres, *J. Porphyrins Phthalocyanines*, **2014**, *18*, 50; d) W. Imhof, A. Sterzik, S. Krieck, M. Schwierz, T. Hoffeld, E. T. Spielberg, W. Plass, N. Patmore, *Dalton Trans.*, **2010**, *39*, 6249.

[2] a) S. Goberna-Ferrón, B. Peña, J. Soriano-López, J. J. Carbó, H. Zhao, J. M. Poblet, K. R. Dunbar, J. R. Galán-Mascarós, *J. Catalysis*, **2014**, *315*, 25; b) M. E. Harvey, D. G. Musaev, J. Du Bois, *J. Am. Chem. Soc.*, **2011**, *133*, 17207; c) L. Villalobos, J. E. B. Paredas, Z. Cao, T. Ren, *Inorg. Chem.*, **2013**, *52*, 12545; d) N. Komiya, T. Nakae, H. Sato, T. Naota, *Chem. Commun.*, **2006**, 4829; e) L. Villalobos, Z. Cao, P. E. Fanwick, T. Ren, *Dalton Trans.*, **2012**, *41*, 644.

[3] a) M. Mikuriya, D. Yoshioka, M. Handa, *Coord. Chem. Rev.*, **2006**, *250*, 2194; b) M. C. Barral, D. Casanova, S. Herrero, R. Jiménez-Aparicio, M. R. Torres, F. A. Urbanos, *Chem. Eur. J.*, **2010**, *16*, 6203; c) T. E. Vos, Y. Liao, W. W. Shum, J.-H. Her, P. W. Stephens, W. M. Reiff, J. S. Miller, *J. Am. Chem. Soc.*, **2004**, *126*, 11630.

[4] a) F. A. Cotton, C. A. Murillo, R. A. Walton, *Multiple Bonds Between Metal Atoms*, 3rd edn ed., Springer Science and Business Media, Inc., New York, **2005**; b) T. Ren, *Coord. Chem. Rev.*, **1998**, *175*, 43; c) T. R. Brown, B. S. Dolinar, E. A. Hillard, R. Clérac, J. F. Berry, *Inorg. Chem.*, **2015**, DOI: 10.1021/acs.inorgchem.1025b01241.

[5] G. M. Chiarella, F. A. Cotton, C. A. Murillo, K. Ventura, D. Villagrán, X. Wang, *J. Am. Chem. Soc.*, **2014**, *136*, 9580.

[6] a) Z. Cao, B. Xi, D. S. Jodoin, L. Zhang, S. P. Cummings, Y. Gao, S. F. Tyler, P. E. Fanwick, R. J. Crutchley, T. Ren, *J. Am. Chem. Soc.*, **2014**, *136*, 12174; b) B. Xi, I. P.-C. Liu, G.-L. Xu, M. M. R. Choudhuri, M. C. DeRosa, R. J. Crutchley, T. Ren, *J. Am. Chem. Soc.*, **2011**, *133*, 15094; c) W. P. Forrest, Z. Cao, K. M. Hassell, B. M. Prentice, P. E. Fanwick, T. Ren, *Inorg. Chem.*, **2012**, *51*, 3261.

[7] a) A. K. M. Long, R. P. Yu, G. H. Timmer, J. F. Berry, *J. Am. Chem. Soc.*, **2010**, *132*, 12228; b) G. H. Timmer, J. F. Berry, *Chem. Sci.*, **2012**, *3*, 3038.

[8] a) S. Herrero, R. Jiménez-Aparicio, J. Perles, J. L. Priego, F. A. Urbanos, *Green Chem.*, **2010**, *12*, 965; b) S. Herrero, R. Jiménez-Aparicio, J. Perles, J. L. Priego, S. Saguar, F. A. Urbanos, *Green Chem.*, **2011**, *13*, 1885.

[9] F. A. Cotton, T. Ren, *Inorg. Chem.*, **1991**, *30*, 3675.

[10] K. M. Kadish, B. Han, J. Shao, Z. Ou, J. L. Bear, *Inorg. Chem.*, **2001**, *40*, 6848.

[11] C. Lin, T. Ren, E. J. Valente, J. D. Zubkowski, E. T. Smith, *Chem. Lett.*, **1997**, 753.

[12] P. Angaridis, F. A. Cotton, C. A. Murillo, D. Villagrán, X. Wang, *Inorg. Chem.*, **2004**, *43*, 8290.

[13] M. C. Barral, R. Jiménez-Aparicio, E. C. Royer, F. A. Urbanos, *Polyhedron*, **1991**, *10*, 113.

[14] a) B. Han, J. Shao, Z. Ou, T. D. Phan, J. Shen, J. L. Bear, K. M. Kadish, *Inorg. Chem.*, **2004**, *43*, 7741; b) M. C. Barral, S. Herrero, R. Jiménez-Aparicio, M. R. Torres, F. A. Urbanos, *J. Organomet. Chem.*, **2008**, *693*, 1597.

[15] M. Manowong, B. Han, T. R. McAloon, J. Shao, I. A. Guzei, S. Ngubane, E. V. Caemelbecke, J. L. Bear, K. M. Kadish, *Inorg. Chem.*, **2014**, *53*, 7416.

[16] a) M. A. S. Aquino, *Coord. Chem. Rev.*, **1998**, *170*, 141; b) M. A. S. Aquino, *Coord. Chem. Rev.*, **2004**, *248*, 1025; c) R. Gracia, H. Adams, N. J. Patmore, *Dalton Trans.*, **2009**, 259; d) E. V. Dikarev, A. S. Filatov, R. Clérac, M. A. Petrukhina, *Inorg. Chem.*, **2006**, *45*, 744.

[17] a) M. A. Castro, A. E. Roitberg, F. D. Cukiernik, *Inorg. Chem.*, **2008**, *47*, 4682; b) O. V. Sizova, L. V. Skripnikov, A. Y. Sokolov, O. O. Lyubimova, *J. Struct. Chem.*, **2007**, *48*, 28; c) R. Gracia, H. Adams, N. J. Patmore, *Inorg. Chim. Acta*, **2010**, *363*, 3856.

[18] M. A. Castro, A. E. Roitberg, F. D. Cukiernik, *J. Chem. Theory Comput.*, **2013**, *9*, 2609.

[19] a) R. Gracia, N. J. Patmore, *Dalton Trans.*, **2013**, *42*, 13118; b) G. H. Timmer, J. F. Berry, *C. R. Chimie*, **2012**, *15*, 192.

[20] M. Costas, M. P. Mehn, M. P. Jensen, L. Que Jr., *Chem. Rev.*, **2004**, *104*, 939.

[21] P. L. Holland, *Dalton Trans.*, **2010**, *39*, 5415.

[22] C. J. Cramer, W. B. Tolman, K. H. Theopold, A. L. Rheingold, *Proc. Natl. Acad. Sci., USA*, **2003**, *100*, 3635.

[23] S.-M. Lee, R. Kowallick, M. Marcaccio, J. A. McLeverty, M. D. Ward, *J. Chem. Soc., Dalton Trans.*, **1998**, 3443.

[24] A. J. Lindsay, G. Wilkinson, M. Motevalli, M. B. Hursthouse, *J. Chem. Soc., Dalton Trans.*, **1985**, 2321.

[25] G. M. Sheldrick, in *A Program for Absorption Correction with the Siemens SMART System*, University of Gottingen, Germany, **1996**.

[26] a) G. M. Sheldrick, *Acta Cryst. Sect. A*, **1990**, *46*, 467; b) *SHELXTL program system version 5.1*, Bruker Analytical X-ray Instruments Inc., Madison, WI, **1998**.

[27] M. J. Frisch, G. W. Trucks, H. B. Schlegel, G. E. Scuseria, M. A. Robb, J. R. Cheeseman, G. Scalmani, V. Barone, B. Mennucci, G. A. Petersson, H. Nakatsuji, M. Caricato, X. Li, H. P. Hratchian, A. F. Izmaylov, J. Bloino, G. Zheng, J. L. Sonnenberg, M. Hada, M. Ehara, K. Toyota, R. Fukuda, J. Hasegawa, M. Ishida, T. Nakajima, Y. Honda, O. Kitao, H. Nakai, T. Vreven, J. A. Montgomery, Jr., J. E. Peralta, F. Ogliaro, M. Bearpark, J. J. Heyd, E. Brothers, K. N. Kudin, V. N. Staroverov, R. Kobayashi, J. Normand, K. Raghavachari, A. Rendell, J. C. Burant, S. S. Iyengar, J. Tomasi, M. Cossi, N. Rega, J. M. Millam, M. Klene, J. E. Knox, J. B. Cross, V. Bakken, C. Adamo, J. Jaramillo, R. Gomperts, R. E. Stratmann, O. Yazyev, A. J. Austin, R. Cammi, C. Pomelli, J. Ochterski,

R. L. Martin, K. Morokuma, V. G. Zakrzewski, G. A. Voth, P. Salvador, J. J. Dannenberg, S. Dapprich, A. D. Daniels, O. Farkas, J. B. Foresman, J. V. Ortiz, J. Cioslowski and D. J. Fox, Gaussian 09 (Revision D.01), Gaussian, Inc., Wallingford, CT, **2013**.

[28] a) A. D. Becke, *Phys. Rev. A*, **1988**, *38*, 3098; b) A. D. Becke, *J. Chem. Phys.*, **1993**, *98*, 5648.

[29] a) J. P. Perdew, K. Burke, M. Ernzerhof, *Phys. Rev. Lett.*, **1996**, *77*, 3865; b) J. P. Perdew, K. Burke, M. Ernzerhof, *Phys. Rev. Lett.*, **1997**, *78*, 1396.

[30] D. Andrae, U. Haeussermann, M. Dolg, H. Preuss, *Theor. Chim. Acta*, **1990**, *77*, 123.

[31] W. J. Hehre, L. Radom, P. v. R. Schleyer and J. A. Pople, *Ab initio Molecular Orbital Theory*, John Wiley & Sons, New York, **1986**.

[32] a) R. E. Stratmann, G. E. Scuseria, M. J. Frisch, *J. Chem. Phys.*, **1998**, *109*, 8218; b) R. Bauernschmitt, R. Ahlrichs, *Chem. Phys. Lett.*, **1996**, *256*, 454; c) M. E. Casida, C. Jamorski, K. C. Casida, D. R. Salahub, *J. Chem. Phys.*, **1998**, *108*, 4439.